shape of the extreme ultraviolet bump which is implied by the available data. This is all the more regrettable since the largest contributions to the total luminosity could come from this bump at least at certain epochs. (At other epochs, the luminosity is probably dominated by the hard X-ray emission, up to a few 100's keV).

The flux variations observed in the different bands imply changes in the spectral parameters. The January 1986 spectrum is thus significantly flatter in the far infrared-mm (down to $\approx 5-10\ \mu m$) domain than the 1984 spectrum, whereas the near infrared emission (between $\approx 1\ \mu m$ and $\approx 5\ \mu m$) remained very stable (3). The slope of the X-ray emission remained, however, nearly constant when the flux changed.

The data we have collected can be used to test theoretical model predictions; they are, however, still far too scarce to constrain the models sufficiently to provide a univocal description of the quasar phenomenon. The complex pattern of time variations also provided evidence for a new spectral component: The different (and unexpected) behaviour observed in the mm-infrared domain above $\approx 5-10\ \mu m$ and below this limit (3) showed that the near infrared emission cannot be dominated by the high energy tail of the far infrared

component, which is generally thought to be of synchrotron origin. The near infrared emission must therefore have an origin of its own, which we do not understand yet. Another example of different time variability patterns is found in the mm-infrared and the X-ray domains: No large mm-infrared flux variations were observed at the beginning of the campaign while the X-ray flux decreased by a factor ≈ 2. This implies that these two components cannot be emitted by the same electron population, as has often been proposed in the so-called synchrotron self-Compton models.

The time scales of variability in the different bands give useful limits to the size of the respective emission regions provided that no relativistic bulk motion or gross projection effects introduce large correction factors. The sizes we can infer from our observations indicate that the hard X-ray emitting region is of the order of ≈ 1 light month, similar to the near infrared emitting region (provided that the dip we observed is confirmed). The variations seen in the ultraviolet domain prior to our observations (4) also indicate a similar size for the region emitting the (optically thick) blue bump. The variations observed in the far infrared imply a size of less than a few light months. This latter number

however cannot be further precised, because of the undersampling of the light curve.

The very different time variation patterns observed in the different bands and the typical variability time scales of ≤ 1 month show the need for numerous more coordinated observations of quasars covering the entire spectrum to reveal the interplay of the different components. Such observing campaigns are difficult to organize as they imply many different observatories around the world and little structure is available to coordinate observations from different institutions. EXOSAT has now finished its life and will not be followed by a European X-ray observing facility for some years. We hope, however, to have access to data from the Japanese X-ray satellite Astro-C to be launched next year to continue our efforts.

References:
1. Courvoisier, T.J.-L., Turner, M., Robson, E.I., Gear, W.K., Staubert, R., Blecha, A., Bouchet, P., Falomo, P., Valtonen, M. and Teräsranta, H., 1986, in preparation.
2. Courvoisier, T.J.-L., 1984, *The Messenger* **37,** September 1984.
3. Robson, E.I., Gear, W.K., Brown, L.M.J., Courvoisier, T.J.-L., Smith, M.G., Griffin, M.J. and Blecha, A., 1986, *Nature*, in press.
4. Courvoisier, T.J.-L. and Ulrich, M.H., 1985, *Nature* **316,** 554.

Modelling Space Telescope Observations

M. ROSA* and D. BAADE, The Space Telescope European Coordinating Facility,
European Southern Observatory

1. Introduction

A software package designed to simulate observations obtained with the Hubble Space Telescope (HST) has been developed at the Space Telescope European Coordinating Facility (ST-ECF) at ESO, Garching. This report presents a comprehensive description of the reasoning and scientific, technical and operational background that has led to the development of this HST Model. Examples illustrate how the model is used to predict the actual results of observations.

2. Technical and Scientific Background

2.1. Operational differences between ground-based and HST observing

Observing experience cannot be gathered from handbooks and users

guides alone. In the case of ground-based observations, it usually is the result of experiments under real observing conditions.

Often the best instrumental set-up and observational procedure is found only after several trials using mediocre atmospheric conditions to prepare for the really good nights.

In view of the expensive observing time and tight scheduling requirements, such a procedure is prohibitive for Hubble Space Telescope (HST) observations (and also not really desirable for ground-based activities). Furthermore, in the case of HST, almost all programmes will be pushing to the absolute limits of feasibility. In order to assure the utmost scientific return it will not be enough to tune the data reduction software to the limits set by information theory. The observational procedures as well will have to be set up in the most efficient way in order to keep the noise level in the data acquired below the largest tolerable value yet spending

the lowest possible amount of the precious observing time allocated.

The optimal use of the HST and its scientific instruments for a given scientific problem will (in general) not be obvious to judge from the technical details of the performance alone. Slight changes in the performance of a given part of an instrument might in fact call for a revision of the entire observational strategy, e.g. the choise of grating and detector combination.

It follows that a system capable of simulating observations with the instruments of HST in advance of the layout of proposals and of the real observations can largely compensate for the lack of experience and of the possibility of interaction in operational procedures.

2.2. Technical differences between dedicated space experiments and HST

Usually astronomical space experiments work in frequency domains inac-

* Affiliated to the Astrophysics Division, Space Science Department, European Space Agency.

cessible from ground and therefore employ telescopes and detectors of highly specialized nature with a very limited range of possible instrumental configurations. Examples are the X- and Gamma-ray experiments and the International Ultraviolet Explorer (IUE), which are free flying laboratory set-ups rather than orbiting versions of ground-based observatories. The IUE for example acquired thousands of exposures in only 4 well-defined, rigidly-fixed spectrographic modes. In such experiments, once the first few raw data are obtained of standard targets, a preliminary instrumental calibration can be produced. This will serve as a means of estimating exposure times and performance for all future exposures to be made of a given type of object.

The (prospective) user of the HST observatory will have to choose between 6 scientific instruments, each of which has a multitude of configurations. Recall that there are two imaging instruments, the Wide-Field and Planetary Camera (WFPC) and the Faint-Object Camera (FOC); two spectrographs, the High-Resolution Spectrograph (HRS) and the Faint-Object Spectrograph (FOS); a High-Speed Photometer (HSP) and the Fine-Guidance Sensor (FGS). The instruments cover the entire wavelength range from 1000 Å to about 1 micron or parts thereof, although with greatly varying efficiencies. The WFPC deploys 8 CCD chips in two focal ratio configurations, 42 filters, 3 polarizers and 3 objective gratings. The FOC consists of 2 intensified photon counting systems imaging at 3 focal ratios with the possibility to insert up to 4 out of 49 different filters, plus one each of 2 polarizers and 5 objective prisms. Spectroscopy with the HRS can be done with two Digicons and 8 gratings with resolutions of 2×10^3, 2×10^4 and 10^5. The FOS also uses two Digicons and offers 6 gratings in medium, 3 gratings or prisms in low resolution mode and spectropolarimetry. HSP consists of 4 image dissector tubes and a photomultiplier, 18 filters, 4 polarimetric filters and an aperture plate with 50 apertures. Finally, the 3 FGS sensors, besides their task of tracking HST during exposures with the other 5 instruments, can perform astrometry in selected wavebands. For more details see the HST Instrument Handbooks and the Call for Proposals distributed by the Space Telescope Science Institute, Baltimore (STScI).

Altogether there are several hundreds of useful modes that can be selected with HST, not including choices to be made for the read-out parameters of the detectors and the freedom in selecting a continuum of central wavelengths for HRS. Simulated HST observations can

provide substantial help for the decision among apparently equivalent but slightly different modes to be selected for a given scientific objective. Finally, only the frequently used modes will be covered by the routine calibration process devised for HST operations. It will therefore be most interesting, if not necessary, to obtain a best guess of the performance in the uncalibrated modes through simulations.

2.3. Differences in performance between HST and ground-based telescopes

The detectors and instruments of HST and the observational techniques are generally well known from ground-based observatories. What makes observing with HST so exceptional is its capability to work near the diffraction limit of its 2.5-m mirror since there is no intervening turbulent atmosphere. In addition, the background light, which is already significantly lower because of operation above the earth's atmosphere, is greatly diminished (for point sources) by the gain in spatial resolution of at least a factor of 7 squared, i.e., per area of the PSF the background contamination is suppressed by another factor of 50.

The new side-effects encountered will for instance be the variation of spatial resolution with wavelength (by nearly an order of magnitude over the accessible wavelength range). This will cause variable throughput for the smallest spectrographic and photometric apertures, a variation of image size with effective colour for stars observed through broadband filters, especially in the UV where red leaks are very disturbing, and, finally, a severe undersampling of the point spread function at short wavelengths in some of the cameras. For ground-based observations, these effects are under most circumstances negligible. Further, due to the lack of a sufficient sky signal level, preflashing of the WFPC CCDs is needed in order to overcome the severe nonlinearity (deferred charge) at low levels of non-uniform illumination with high spatial frequencies. Finally, faint (undersampled) stars in Wide-Field Camera images may not be distinguishable from weak cosmic ray events because both signals will produce significant amounts of charge in only a very few detector elements.

In conclusion, we stress that it is the combination of the characteristics of astronomical targets in the spatial and spectral regimes with the performance of HST that makes the acquisition of an a priori experience so indispensable for the preparation of valuable observations and for their subsequent processing.

3. The Model Package

Conceptually, a realistic simulation of astronomical observations is nothing else but an inversion of the data reduction path. The latter consists of, e.g., resampling from pixel to wavelength domain, deconvolution with instrumental profiles, extinction corrections and calibration with instrumental sensitivities. Instead, the modelling software will start with a clean target (image or energy distribution), will then modulate the signal by including interstellar extinction, redshift, etc. and deteriorate it further by applying all the effects intrinsic to the assumed instrumental setup. The latter include for example the point spread function, dispersion relation, filter transmission, detector sensitivity, intensity transfer function, scattered light, photon statistics and detector noise. A model package will have to be very modular in order to provide flexibility at the input stage, i.e. the generation of astronomical targets and to remain adaptable to new instruments, configurations and changes of technical data.

It seemed natural to develop the model as a package of application programmes, data bases and command language level procedures embedded in the environment of the large astronomical data analysis system MIDAS produced and maintained at ESO (see Banse et al., *The Messenger*, No. 31, p. 26, 1983). This concept results in several advantages. Firstly, only a very few highly specialized FORTRAN level programmes had to be written from scratch, while all the data handling, display, hardcopy and image arithmetics needed was already covered by MIDAS system commands. Secondly, knowledge of the instrument configurations could be maintained in the model in the form of look-up tables, and the flow chart of the photons through the instruments in the form of command procedures which activate individual system commands. This scheme provides for easy debugging, updating and upgrading. Thirdly, the astronomical data (e.g. extinction tables, sample spectra and images) needed for the target generation are stored in an expanding data base accessible to all MIDAS users. Finally, any addition of application programmes to the general MIDAS system or to the HST Model package will be beneficial for the users of either software environment.

The model is structured into 3 major components, namely TARGET GENERATION, OPTICAL PATH and DETECTION. Targets as seen at the entrance pupil of HST come in three major flavours, i.e. 2 D images, point source
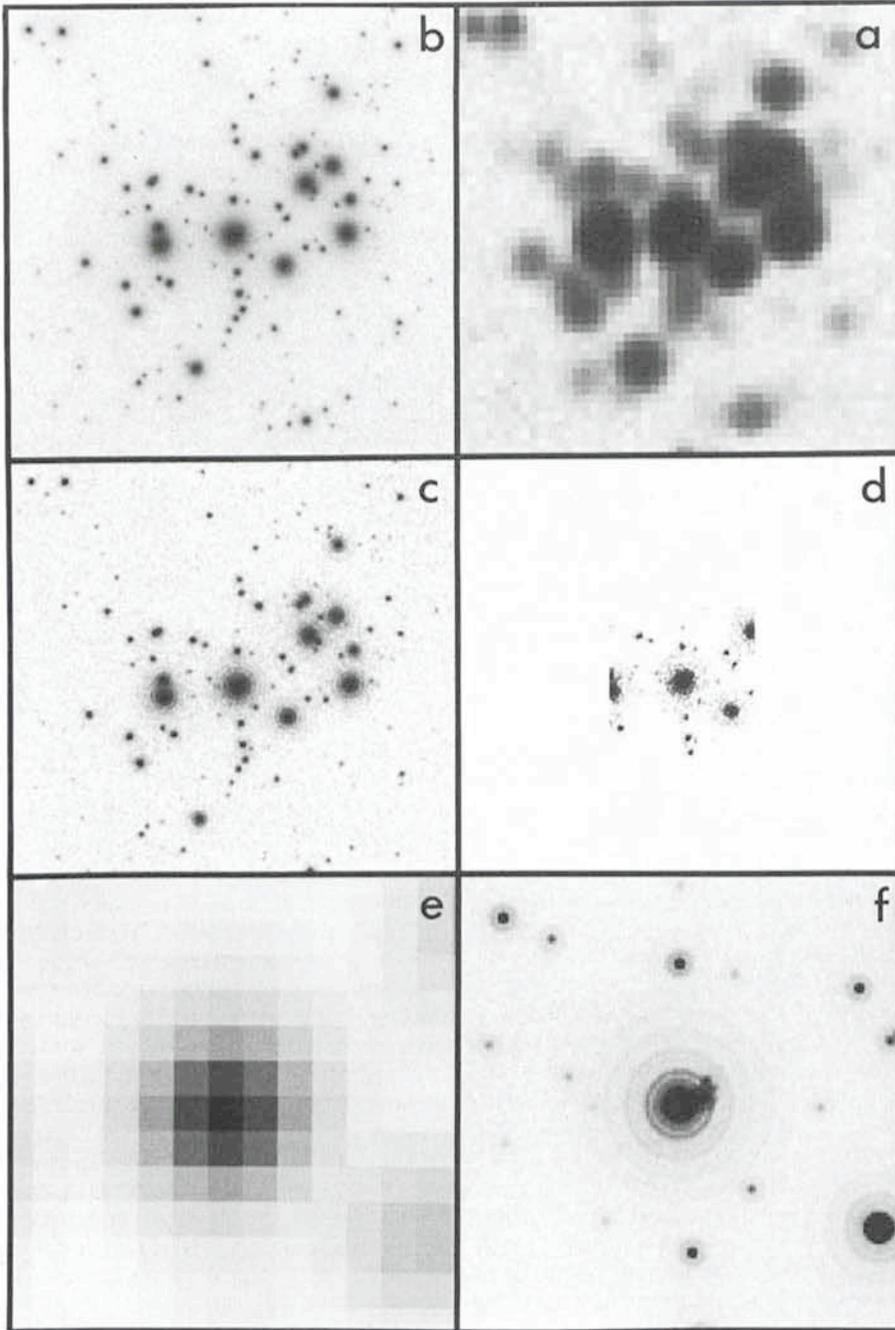
Figure 1: *Simulated images of the Pleiades at 120 kpc distance. (a) ESO 3.6 m, prime focus CCD, seeing 0.5 arcsecond, 3 minutes. (b) FOC f/48 (= PC), (c) FOC f/96 and (d) FOC f/288 — all exposed for 1,000 seconds through B filter, (e) and (f) are enlargements of the central parts of (a) and (d).*

pixel variation of these parameters for the different detectors.

Several data bases are provided with the package. An ASTROPHYSICAL DATA BASE contains extinction tables, spectral catalogues with low and high resolution sample spectra, model atmospheres, images of galaxies, star clusters, H II regions and planetary nebulae, and line lists for emission-line objects. The HST INSTRUMENT DATA BASE comprises for example filter transmissions, detector efficiencies, dispersion relations, intensity transfer functions and flat fields, the HST DATA BASE mirror reflectivities and point spread functions. Astronomical targets and results generated by the users are archived and provide a growing data base for further applications.

In summary, the model package performs the following tasks:

1. Creation and modification of realistic astronomical targets, based on real and/or artificial data.
2. Observation of these targets with different instrumental configurations.
3. Acquisition of data including the peculiarities of the detectors.
4. Use of the general MIDAS environment to modify, hardcopy and analyze the data at any intermediate step.

4. Examples

In the remainder of this article we present some examples obtained with the model package. Rather than discussing all the details of a particular case we emphasize the differences between ground-based experience and expected HST results. More details on the HST PSF and sampling problems can be found in papers by King (1979; *PASP* **95,** 163) and Bendinelli, Di Iorio, Parmeggiani and Zavatti (1985; *AA* **153,** 265), on the appearance of WFPC images of Local Group galaxies in a paper by Hoessel and Danielson (1985; *PASP* **95,** 336).

4.1. The Pleiades at 120 kpc distance

Figure 1 shows artificial images of an open cluster that has been generated using the brightest 300 members of the Pleiades but scaled in position and brightness to a distance of 120 kpc. This distance, in fact about 2 times the LMC distance, has been chosen in order to squeeze the cluster into the field of the FOC f/96 mode. Note that no additional field stars have been added and that a flat background of 25 mag per square arcsec has been assumed. The brightest star mapped has a B magnitude of 17 mag, the faintest ones are at about 29 mag and contribute only statistically to a slightly enhanced
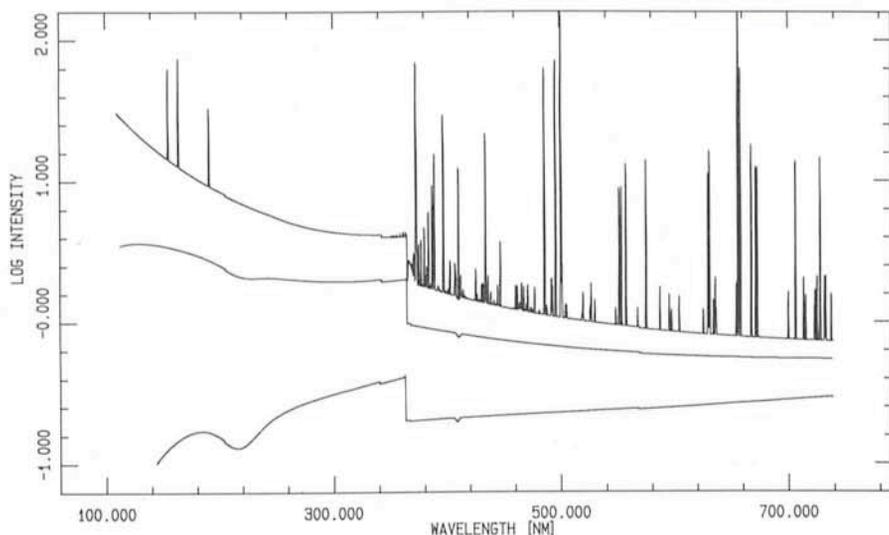
catalogues and energy distributions. In principle, a target will be a multi-dimensional data entity providing monochromatic irradiance as a function of position, wavelength and time. Sampling intervals and size in either of the 3 domains will depend on the particular instrument configuration chosen and the analysis to be performed. For example, targets for imaging will be rather large in the spatial domain but will be sparsely sampled in the wavelength regime, while targets for spectroscopy will eventually carry no spatial information at all but will have a very good resolution in the spectral domain. Target generation

includes also various backgrounds, redshifting, reddening and scaling in space and photon flux.

The optical path includes all effects encountered between the HST orbit (e.g., scattered light from sun, moon, and earth, airglow, Doppler shift, aberration) and the detectors (e.g. reflectivities of mirrors, filter transmissions, dispersion relations, geometric distortions, point spread functions). Finally, the actual acquisition of the data (DETECTION) is handled in specific modules that include particle events, intensity transfer functions, quantum effficiencies, read out noise, and the pixel-to-

Figure 2: *Simulated spectrum of a planetary nebula. The effect of interstellar extinction on the continuum is shown for an LMC extinction law at E (B−V) = 0.15 and 0.5 mag, respectively.*

4.2. FOS spectra of a faint planetary nebula in the LMC

Figure 2 shows the modelled energy distribution of a planetary nebula plus its central star in the LMC, m (B) = 20 mag. We used a 100,000 K black body, the relative emission-line strengths of NGC 7027 and a nebular emission continuum, all ingredients properly scaled for an observation in a 0.5 arcsec aperture. In addition, a weak H(gamma) absorption line has been added as an example of the stellar absorption spectrum. Two continua without nebular emission lines have been drawn for interstellar extinction in the LMC with E (B−V) = 0.015 and = 0.5, respectively. A scientific objective of these simulations would be the evaluation of the best instrumental configurations and the exposure times required for a proper analysis of such objects with the Faint Object Spectrograph.

Figure 3 shows the count-rates obtained for the input spectrum with E (B−V) = 0.15 in the low resolution modes G 160 L plus blue digicon and G 650 L plus red digicon, respectively. The figure also makes the missing spectral coverage of the region between 240 and 380 nm by the FOS in its low resolution mode quite evident. A fully-fledged simulation is presented in Figure 4 where the final "raw observational" data of a 1,000 second integration using grating G 400 H and the blue digicon is shown. Note that at this spectral resolution and with the signal-to-noise ratio (SNR) obtained, the broad absorption underlying the H-gamma emission is invisible.
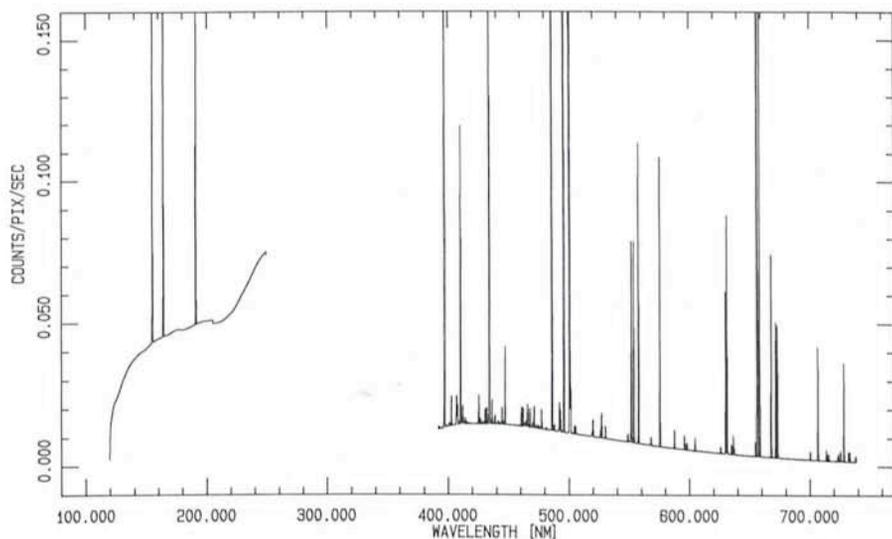
background level. Figure 1a shows a 180-second integration on a CCD mounted at the prime focus of a 4-m class telescope. A gaussian seeing profile of 0.5 arcsec FWHM has been assumed. Figures 1b through 1d show Planetary Camera (or FOC f/48), FOC f/96 and FOC f/288 images. Exposure times would have been 1,000 seconds each through B band filters. Figure 1e and 1f zoom in on the image of the brightest star in the centre of the cluster as seen from the ground and in the FOC f/288 mode, respectively. In interpreting "excellent-seeing" ground-based images of mysterious objects, i.e. R 136a in 30 Doradus, one may occasionally wish to compare these two images. They demonstrate how much structure can be hidden behind a 0.5 arcsec seeing profile and a high background level.

Fairly obvious is the increase in resolution but more interesting at this point is the notable undersampling of stellar images in the PC or FOC f/48 frames (even more severe for WF). In the extreme case (WF) a blue PSF of 0.02 arcsec FWHM is sampled with pixels of 0.1 arcsec width, leading to triangular, square, or bar-shaped images of faint stars with only 1 to 4 significant pixels. A pre-requisite for successful application of photometry packages that employ scaling of a PSF to measure magnitudes in crowded stellar fields (eg. DAOPHOT) will be the acquisition of multiple frames slightly shifted by fractions of a pixel size with respect to each other (in order to satisfy the Nyquist theorem in two dimensions). Note also the fringing of bright stars, the exact pattern of which will depend on effective wavelength in broad bandpass filters. Point spread functions of HST and associated problems have also been discussed recently

by Bendinelli, Di Iorio, Parmeggiani and Zavatti (1985; *AA* **153,** 265).

Since we used a point symmetric PSF and did not include the diffraction pattern of the spiders, speckle patterns due to misalignments and non-ideal mirror figures, scattering by microroughness and dust on the mirrors, one should consider the images of the brighter stars only as the currently best guess of what an azimuthal average over a stellar image would look like. This is especially true for the FOC f/288 mode. Laboratory simulations of speckle images in the f/288 mode have been presented by Lohmann and Weigelt (ESA/ESO Workshop on "Astronomical Uses of the Space Telescope", F. Macchetto, F. Pacini and M. Tarenghi (eds.), ESO, 1979, p. 353) and Weigelt (ESO Conference on the "Scientific Importance of High Angular Resolution at Infrared and

Figure 3: *Count rates in FOS modes G 160 L (blue digicon) and G 650 L (red digicon) using as input the spectrum with E (B−V) = 0.15 mag from Figure 2.*
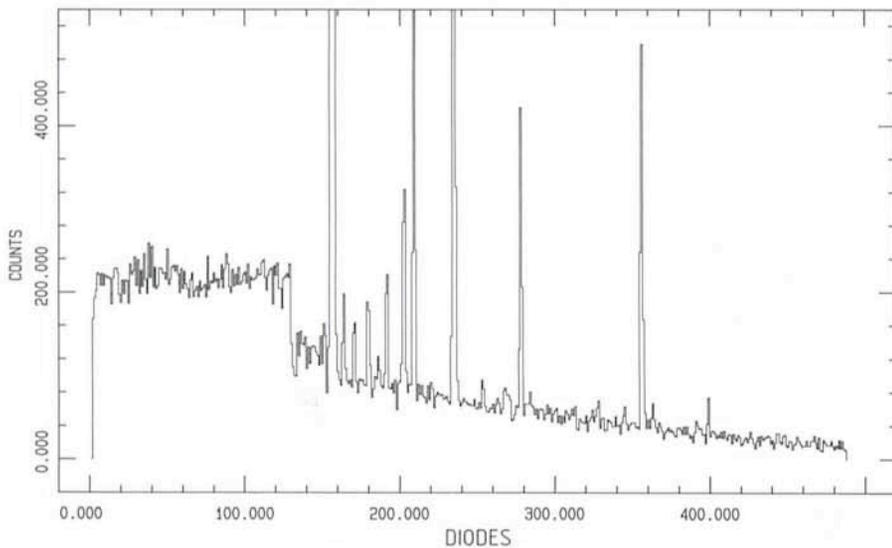
Figure 4: *Raw data acquired in 1,000 seconds in FOS mode G 400 H (blue digicon) using the same input as in Figure 3.*

extreme rates quickly drops to zero. This happens long before a lethal level of the illumination is reached. Therefore, depending on the amount of background, even a faint star can actually lead to critical count rates. In Figure 5 we demonstrate this effect for a binary with 0.2 arcsec separation and an intensity ratio of 1/1,000. The top panel displays a cut through the image in photon flux units at the detector (FOC f/288, effective wavelength 170 nm, 256 * 256 pixels), the wiggly wings of the bright stars profile stem from the diffraction pattern which is almost unresolved at this wavelength. The lower panel shows from bottom to top 1,000 sec. integrations through various combinations (as labelled) of the medium bandpass F 170 M filter and neutral density filters
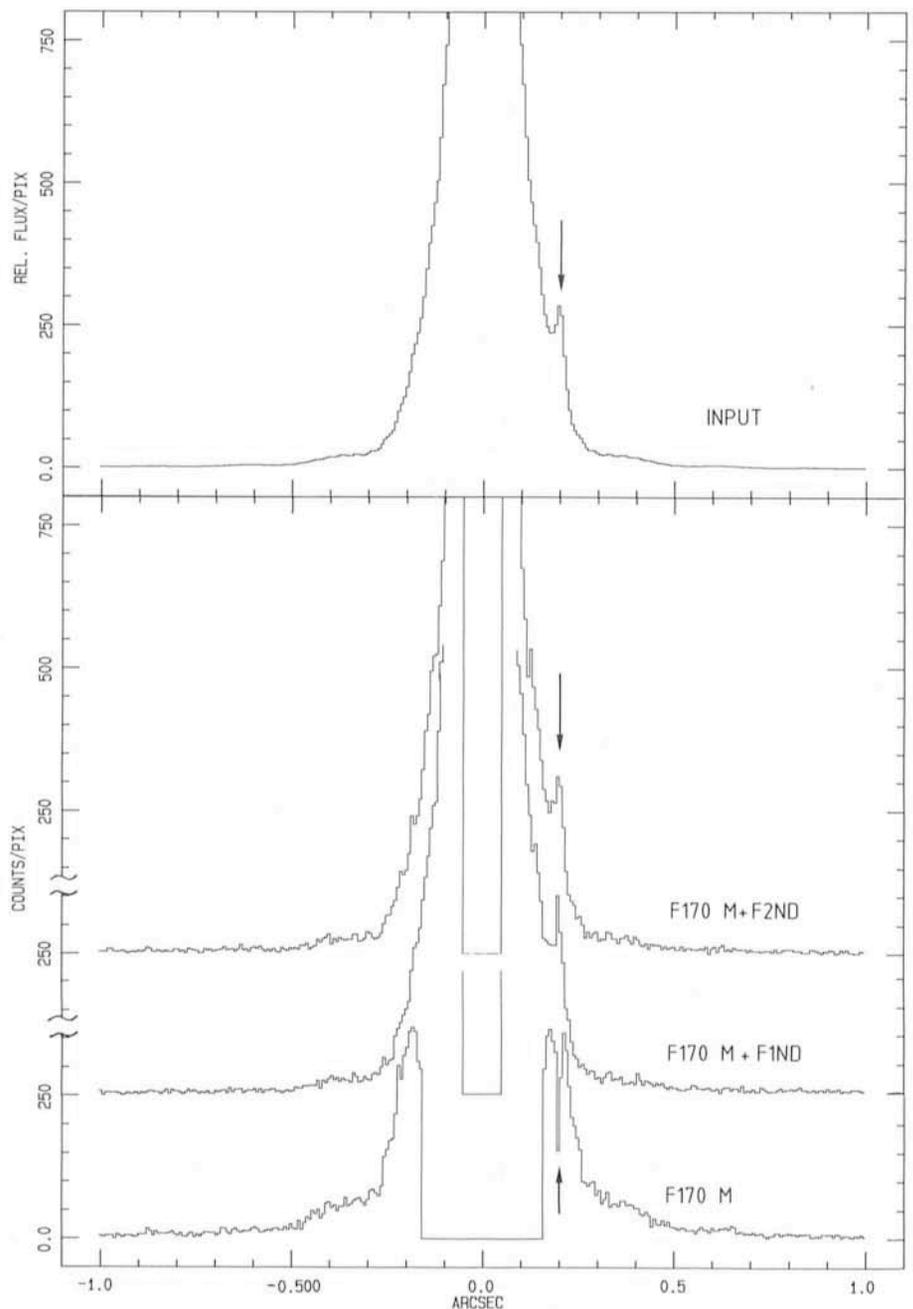
The simulations demonstrate clearly the variability of the SNR over the free wavelength range. Furthermore, the assumption that the performance for hot stars is increasing with decreasing wavelength is extremely dependent on the amount of extinction that has to be expected towards the object. Finally, it is noteworthy that in the visual wavelength range the faint object spectrograph EFOSC at the 3.6-m telescope of ESO, La Silla, produces a similar SNR for objects of about 19 mag (B) in 3,600 sec. i.e., only 2.6 times more exposure time.

4.3. Close double stars with a large brightness ratio

The last example focusses on a challenging application of the high-resolution imaging offered by HST in combination with the FOC f/288 imaging mode. Taking the theoretical FWHM (in pixels) of stellar images in the f/288 mode given in the manuals at face value, the detection and resolution of stellar pairs with separations of 0.2 arcsec should be no problem at all. However, if the brightness of the stars differs too much, the (noisy) diffraction pattern of the bright component will render the faint one invisible. To reach this conclusion does not really require simulated observations, but the latter might help to optimize the selection of the bandpass in such a way that the faint component will not be burried in a strong diffraction feature. Yet there is still another effect that has to be considered when estimating exposure times. The intensity transfer function (ITF) of the FOC becomes very nonlinear at typical count rates above 0.6 cts/s/pixel, depending on the actual configuration chosen. The ITF then levels off (saturation) and at more

Figure 5: *Slices through FOC f/288 images of a double star with a separation of 0.2 arcsecond and brightness ratio 1/1,000. See section 4.3 for more details.*

of 1 and 2 mag attenuation. Since the example is chosen in such a way that the wings of the bright star are already close to nonlinearity, the SNR in the wings does not change dramatically with the choice of filters. The core of the bright star is therefore always beyond saturation, i.e. at zero level. Note the behaviour of the faint star. Without attenuation it is also subject to oversaturation, i.e., is represented by a hole in the wings of the bright star's image because the faint star's flux is added to this very high background. Adding stronger and stronger attenuating filters actually increases the detectability: With a 2 mag density filter in the beam, the SNR is superior to the 1 mag combination.

This last example demonstrates nicely, how much experience can be gained from mere simulations. Obviously, there will always be observations that reveal the unpredicted and therefore cannot be anticipated during simulations. What can be learned, however, is the awareness of problems that may be unimportant under certain circumstances (which usually are not encountered by most ground-based observing programmes) but can determine completely the outcome of another type of observation.

5. Availability

The model package is available for use at the ST-ECF, ESO, Garching. On-line help facilities, a Users Guide and documentation of the Data Bases are provided. Although its main purpose is to simulate HST observations, it can easily be adapted to other instrumentations as well, and we anticipate that the instrumental data of cameras, filters and spectrographs in operation at ESO, La Silla, will become available. Prerequisits for a successful use of the model are experience with the MIDAS system, a detailed prescription of the astronomical target to be generated and familiarity with the HST Instrument Users Guides applicable. A minimum of 3 days should be allocated for a typical project. Prospective users should contact the ST-ECF for details, arrangements of staff support and booking of computer time.

NEWS ON ESO INSTRUMENTATION

The ESO TV Autoguiders

M. DUCHATEAU and M. ZIEBELL, ESO

In February 1985 four new autoguider systems have been installed at La Silla. The 3.6-m telescope, the CAT, the 2.2-m telescope and the Schmidt got equipped with a system.

They have been used now successfully for one and a half year and we hope that they are not "job killers" but that in the meantime they have been accepted as an improvement of work conditions.

Three main reasons induced us to use low-light-level TV cameras for autoguiding:

1. There were already 5 telescopes at La Silla equipped with TV cameras for manual guiding.

2. An electronic crosshair already existed and by setting several electronic signals for it the development of the autoguider was simplified.

3. Long experience with manual guiding on the Schmidt telescope's electronic crosshair encouraged us to continue in the same direction. The stability of the deflection system of the TV camera did not create any difficulty.

The idea was therefore to use the video signal of a TV camera in connection with an electronic crosshair as shown in Figure 1:

Except for the TV camera, all the components are installed inside the control consoles. In some locations, the digital memory used for scan conversion in case of an integration facility does not exist. The video signal is then connected directly from the TV camera to the autoguider chassis (Fig. 2). The advantage of this solution is that no mechanical and no optical modifications are needed in the focal plane.

Electronic Crosshair

The electronic crosshair, developed to perform corrections for differential refraction on the Schmidt telescope, produces on the monitor one fixed cross, one movable and a rectangular box around the centre of the movable cross-
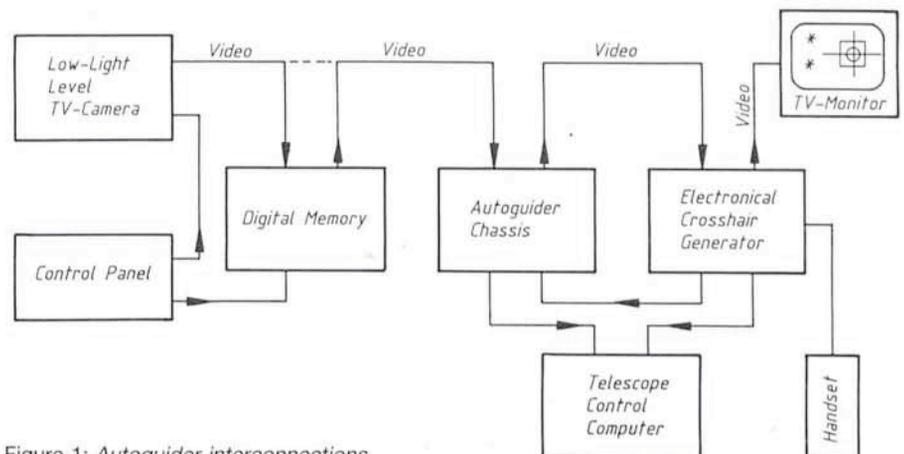

Figure 1: Autoguider interconnections.